# Molecular Dynamics Simulations of the Liquid/Vapor Interface of Aqueous Ethanol Solutions as a Function of Concentration

**Ethan Stewart, Roseanne L. Shields, and Ramona S. Taylor***

*Department of Chemistry, College of the Holy Cross, Worcester, Massachusetts 01610*

*Received: October 4, 2002; In Final Form: January 7, 2003*

Molecular dynamics computer simulations are utilized to study the structural and thermodynamic properties of the liquid/vapor interface of aqueous ethanol solutions as a function of concentration. In addition, the free energy profile for inserting a single ethanol molecule into a 0.059 mole fraction aqueous ethanol solution is calculated using statistical mechanical perturbation theory. The calculated free energy for solvation of an ethanol molecule in the bulk solution, the surface tension as a function of ethanol concentration, and the average orientation of ethanol molecules at the solution/vapor interface are in agreement with the corresponding experimental data. The calculated equilibrium free-energy profile, however, exhibits a barrier to solvation that is considerably smaller than that predicted by the resistance model for mass accommodation.

## I. Introduction

Liquid/vapor interfaces play a key role in many biological, chemical, materials, and environmental processes. For example, gas/liquid interfaces are integral to environmental problems such as the generation of tropospheric ozone, the formation of cloud condensation nuclei, the depletion of stratospheric ozone, water pollution, and acid rain deposition.[1] Due to its intrinsic asymmetry and two-dimensionality, the interface between two bulk systems typically has different chemical and physical properties than either of the bulk systems. It is often more reactive than either bulk medium. It can enhance or impede the occurrence of chemical reactions, and it can mediate the transfer of chemical species between the two bulk systems. The structures of liquid interfaces are much more sensitive to the presence of adsorbed molecules than solid interfaces. Thus, to truly understand how liquid interfaces participate in various chemical processes, we need a molecular-level understanding of those types of forces that dictate the underlying structure of the interface.

The solution/vapor interfaces of aqueous solutions have long been the subject of chemical study. In the early 20th century, surface tension measurements of aqueous alcohol solutions revealed that the alcohol molecules were surface active.[2,3] Today, direct insight into the microscopic structures of the alcohol solution/vapor interface is available via sum frequency generation (SFG) and second harmonic generation (SHG) spectroscopies.[4−7] For example, using SFG, Wolfrum and co-workers measured an excess density of methanol molecules at the solution/vapor interface of aqueous methanol solutions.[7] They found that the molecular ordering of the surface methanol molecules increased as the overall concentration of methanol decreased.[7] Neutron reflectivity measurements provide details into the macroscopic structure of the alcohol−$H_2O$ solution/vapor interface.[8] Li and co-workers have measured the density profiles of both the ethanol and $H_2O$ molecules along the normal to the interface for aqueous ethanol solutions with ethanol mole fractions below 0.24.[8] In addition, they determined both the surface excess of ethanol molecules and the width of this excess.

Classical dynamics simulations are also commonly used to probe the structure of the liquid/vapor interface.[9−19] The information garnered from these types of calculations is complementary to the experimental data described above. Simulations allow one to "see" the structures both of the adsorbed molecules and of the underlying liquid substrate. In the early 1990s, Matsumoto and co-workers performed an in depth study of the solution/vapor interface of aqueous methanol solutions as a function of concentration.[10] In agreement with experiment, this work suggested that methanol preferentially adsorbs at the solution/vapor interface at all methanol concentrations.[10] However, uncertainty existed regarding the actual molecular composition of the surface region in the concentration range of 0.2 to 0.5 mole fraction of methanol. In 1996, Tarek, Tobias, and Klein examined the structural and hydrogen bonding properties of the interface for a 0.1 mole fraction aqueous ethanol solution via molecular dynamics (MD) simulations.[13] They, too, observed the segregation of the alcohol molecules, in this case ethanol, toward the liquid/vapor interface. However, no attempt was made to study the structure of the liquid/vapor interface as a function of bulk ethanol concentration. Mountain examined the composition profiles for the solution/vapor interface of aqueous acetonitrile solutions as a function of concentration.[18] In all cases, acetonitrile was also found to be surface active. Benjamin investigated the thermodynamics, structural, and dynamic properties of the $H_2O$/DMSO solution/vapor interface as a function of DMSO concentration.[12] Although DMSO is a very different molecule than either ethanol or methanol, it again segregated toward the liquid/vapor interface. This segregation, however, was not as substantial as that observed for ethanol. In addition, Benjamin found an enhancement in the fraction of *good* hydrogen bonds per $H_2O$ molecule as the interface was approached. This enhancement was more pronounced for the 0.05 mole fraction DMSO solution than for the 0.20 mole fraction solution. Given the differences in the chemical nature of DMSO and ethanol, it will be interesting to see if this enhancement of the $H_2O$−$H_2O$ hydrogen bonds also occurs in aqueous ethanol solutions.

Aqueous alcohol interfaces have also been useful in advancing our understanding of the process of mass accommodation.[14−16,20,21]

* Corresponding author. E-mail: rtaylor@holycross.edu.

10.1021/jp0271357 CCC: $25.00 
Published on Web 02/13/2003

The interaction of small gas-phase molecules with the liquid/vapor interface of aqueous droplets and their subsequent accommodation into the bulk of the droplet is an integral part of many atmospheric processes.[21] Experimental investigations into mass accommodation predict that the impinging molecule must cross a large energy barrier before becoming solvated, or accommodated, in the bulk liquid.[21] In past work, we have used MD computer simulations to examine the origin of this barrier by simulating the accommodation of a single ethanol molecule by a $H_2O$ droplet.[14,15] However, within the constraints of the experimentally derived resistance model,[21] we were unable to reproduce the experimental results. One assumption of the resistance model is that the impinging molecule interacts with a *clean* $H_2O$ surface.[21] Our simulations and the recent experiments of Donaldson and Anderson[22] question if this is in fact the case. Thus, here we are asking what happens if the impinging ethanol molecule is forced to cross an adsorbed ethanol film before becoming solvated within the bulk $H_2O$.

In this work, we have used the OPLS all-atom (OPLS/AA) potential function for ethanol[26] and the extended simple point charge (SPC/E) potential for $H_2O$[23] in conjunction with MD computer simulations to explore both the structural and thermodynamic properties of the solution/vapor interface of aqueous ethanol solutions as a function of ethanol concentration. The accuracy of any classical simulation is limited by the accuracy of the interaction potential functions employed. Potential functions are available that reproduce many of the bulk properties of pure ethanol and of pure water. Yet, the ability of these potentials to reproduce the interfacial properties of ethanol/water solutions remains undetermined. Comparisons of our simulation data to the corresponding experimental data suggest that the combination of the OPLS/AA and SPC/E potentials both qualitatively and quantitatively describes the thermodynamic and structural properties of the solution/vapor interface of aqueous ethanol solutions. We have also investigated the hydrogen bonding structure of both ethanol and $H_2O$ molecules as a function of their distance from the interface. Unlike the DMSO work of Benjamin,[12] we see no concentration effect on the fraction of *good* hydrogen bonds between $H_2O$ molecules as a function of distance from the interface. Finally, statistical mechanical perturbation theory[32,33] is used to calculate the free-energy profile for inserting an ethanol molecule into a 0.059 mole fraction aqueous ethanol solution. This free-energy profile does not exhibit the barrier to bulk solvation that is predicted by the resistance model.

## II. Method

**A. Potential Model.** The $H_2O$ model employed in these calculations is the rigid SPC/E water potential developed by Berendsen and co-workers.[23] This potential has been shown to adequately reproduce the surface tension and structural properties of the $H_2O$ liquid/vapor interface.[24,25] The all-atom OPLS (OPLS/AA) potential of Jorgensen is used to model the interactions between ethanol molecules.[26] Both of these potential models treat the intermolecular interactions via the combination of a Lennard-Jones 6−12 and a Coulomb potential:

$$U(r_{ij}) = 4\epsilon_{ij}\left[\left(\frac{\sigma_{ij}}{r_{ij}}\right)^{12} - \left(\frac{\sigma_{ij}}{r_{ij}}\right)^{6}\right] + \frac{q_i q_j}{r_{ij}} \qquad (1)$$

where $r_{ij}$ is the distance between atoms $i$ and $j$ in different molecules, $q_i$ is the charge assigned to atom $i$, and $\sigma_{ij}$ and $\epsilon_{ij}$ are the Lennard-Jones parameters. The parameters for the SPC/E and OPLS/AA potentials are given in Table 1. The intermolecular alcohol−$H_2O$ parameters are determined by the Lorentz−Bertholot mixing rules.[27]

**TABLE 1: Intermolecular Lennard-Jones and Coulomb Parameters for SPC/E Water[23] and OPLS/AA Ethanol[26]**

| atom type | $\sigma$ (Å) | $\epsilon$ (kcal/mol) | $q$ (au) |
|---|---|---|---|
| H (water) | 0 | 0 | +0.4238 |
| O (water) | 3.166 | 0.1554 | −0.8476 |
| H (alcohol) | 0 | 0 | +0.418 |
| O (alcohol) | 3.120 | 0.170 | −0.683 |
| C (methylene) | 3.50 | 0.066 | +0.145 |
| C (methyl) | 3.50 | 0.066 | −0.180 |
| H (alkyl) | 2.50 | 0.030 | +0.060 |

**TABLE 2: Summary of System Sizes**

| ethanol mole fraction ($\chi_{ethanol}$) | no. of water molecules | no. of ethanol molecules | x × y × z (Å$^3$) |
|---|---|---|---|
| 0.026 | 1485 | 40 | 36.30 × 36.30 × 108.90 |
| 0.059 | 1285 | 80 | 35.87 × 35.87 × 107.61 |
| 0.11 | 1029 | 130 | 34.86 × 34.86 × 104.58 |
| 0.40 | 1260 | 825 | 48.73 × 48.73 × 146.19 |
| 1.00 | 0 | 488 | 36.21 × 36.21 × 108.63 |

The OPLS/AA potential is a flexible potential that accounts for both the bond stretching, angle bending and torsional interactions. The bond stretching and bending potentials are treated harmonically. The torsional interactions are determined from the following Fourier series:

$$U_{tor} = \sum_i \left\{ \frac{V_1^i}{2}[1 + \cos(\phi_i + f1_i)] + \frac{V_2^i}{2}[1 - \cos(2\phi_i + f2_i)] + \frac{V_3^i}{2}[1 + \cos(3\phi_i + f3_i)] \right\} \qquad (2)$$

Here, $\phi_i$ is the dihedral angle, $V_1$, $V_2$, and $V_3$ are the Fourier coefficients, and $f1$, $f2$, and $f3$ are the phase angles. The total torsional energy is a sum of the torsional energies originating from each torsional angle $i$.

Because the mass accommodation experiments predict the accumulation of only a very small concentration of ethanol in the bulk of the droplet,[20,21] we have chosen to investigate aqueous ethanol solutions with less than 0.50 mole fraction ethanol concentration. We have collected surface tension, structural and dynamical data for four ethanol/water solutions. These solutions, which are described in Table 2, have ethanol mole fractions ($\chi_{ethanol}$) of 0.026, 0.059, 0.11, and 0.40. Each solution is prepared by randomly replacing $H_2O$ molecules in an equilibrated box of SPC/E $H_2O$ with ethanol molecules to give the desired ethanol mole fraction. The newly created bulk aqueous ethanol solution is then equilibrated for 200 ps in a NPT ensemble with a pressure of 1 atm. After the bulk equilibration process is complete, the $z$ dimension of the box is increased by a factor of 3 (as shown in Figure 1) and the new system is equilibrated for an additional 500 ps in a NVT ensemble with no pressure monitoring. The $z$ dimension is now the direction perpendicular to the two newly created solution liquid/vapor interfaces. The $x$, $y$, and $z$ dimensions of these four equilibrated aqueous ethanol solutions, and of a pure ethanol system, are given in Table 2.

No data analysis is performed before the initial 500 ps equilibration is completed. For the surface tension measurements, 10 50 ps trajectories are run in which the data is collected and analyzed. At each concentration, these 10 surface tension values are averaged to give the reported value. After these 10

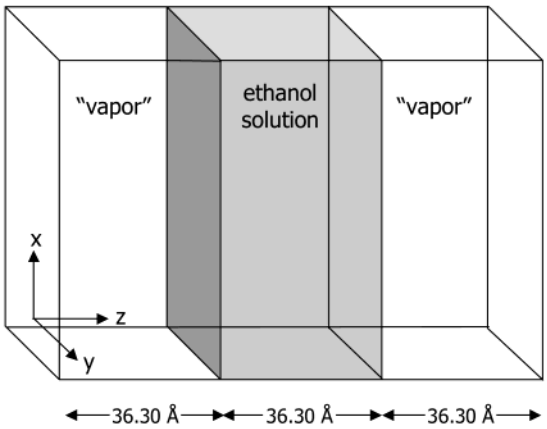


**Figure 1.** Simulation cell for the 0.026 mole fraction aqueous ethanol solution. A rectangular section of an ethanol/$H_2O$ solution is sandwiched between two sections of "vapor". The *z* axis is perpendicular to the two solution/vapor interfaces. The lengths of the box in the *x* and *y* directions are determined from simulations of bulk solutions of the specific concentration of interest. All five ethanol concentrations follow this same format. In all cases, the length in the *z* direction is 3 times the length in the *x* direction. The lengths in the *x*, *y*, and *z* directions are given in Table 2 for all five systems.

trajectories, a 100 ps and a subsequent 200 ps trajectory are run during which the density profiles, orientational, and hydrogen bonding analyses are completed. The results of these two trajectories are compared to ensure that the calculated values are truly equilibrium values.

All of the molecular dynamics simulations are performed using a modified version of the AMBER 4.0 suite of programs.[28] AMBER 4.0 utilizes a Verlet integrator[29] to solve the equations of motion. A step size of 0.001 ps is employed. The temperature of the simulation cells is maintained at 298 K via the Berendsen scheme[30] with a coupling constant of 0.2. All of the bond lengths in both $H_2O$ and ethanol are constrained via the SHAKE algorithm.[31] However, in the ethanol molecules, neither the bond angles nor the torsional angles are constrained. All simulations utilize a cutoff distance of 11 Å.

**B. Potential of Mean Force.** The free-energy curve for the insertion of an ethanol molecule into a 0.059 mole fraction ethanol solution is calculated using the thermodynamic perturbation approach.[32,33] Statistical mechanical perturbation theory has been widely used to calculate the potential of mean force (PMF) for the association of two entities in a bath of solvent molecules.[15,19,34,35] The PMF provides a means to quantify the effect of the bath molecules on the intermolecular interaction of two entities along a reaction coordinate. Here, we have chosen the reaction coordinate to be the distance along the *z* dimension between the centers of mass of a single impinging ethanol molecule and of the box of ethanol and water molecules that constitute the 0.059 mole fraction aqueous ethanol solution. This is a similar approach to that which was utilized in our earlier work, which investigated the free energy for the insertion of a single ethanol molecule into bulk water.[14,15]

The difference in the calculated free energies between two successive steps along the reaction coordinate is equal to the reversible work, $W(z)$, for this configurational change in the presence of the bath. The relative free-energy difference between two configurations is calculated as follows:

$$\Delta A = -RT \ln(\langle \exp\{-[U(z_0 + \Delta z) - U(z_0)]/RT\}\rangle_{z_0}) \quad (3)$$

where $T$ is the temperature of the system. The difference in the Helmholtz free energies, $\Delta A$, is calculated between a reference system, $z_0$, and a system where the reaction coordinate is perturbed from $z_0$ to $(z_0 + \Delta z)$. $U(z_0)$ and $U(z_0 + \Delta z)$ are the potential energies of the reference system and the perturbed system, respectively. $\langle \cdots \rangle_{z_0}$ indicates that the ensemble average is calculated relative to the potential energy of the reference state, $U(z_0)$. This ensemble average includes all of the ethanol and $H_2O$ bath configurations and all of the internal and orientational degrees of freedom of the impinging ethanol molecule that keep the centers of mass fixed. A complete equilibrium free-energy curve (or $W(z)$) as a function of the reaction coordinate is ascertained from a series of such configurations.

Equation 3 is defined in a canonical ensemble (where the number of molecules, volume, and temperature are held constant) and yields a Helmholtz free-energy difference. In the present set of simulations, the total volume of the system is fixed but the free interfaces allow the volume of the liquid phase to fluctuate. Although no external pressure is applied, the free energies calculated from these simulations can be directly compared to the experimentally measured Gibb's free energies because the volume of the aqueous ethanol solution is allowed to fluctuate to accommodate the ethanol molecule as it is inserted.

To determine the equilibrium free-energy curves, $W(z)$, for the accommodation of ethanol by a 0.059 mole fraction aqueous ethanol solution, a series of simulations are performed in which the center-of-mass of an impinging ethanol molecule is moved by 0.5 Å along the reaction coordinate toward the bulk solution. Each simulation is equilibrated for 50 ps prior to a 100 ps trajectory in which energetic data is collected every 0.005 ps. Toward the minimum in the free-energy curve it became necessary to move the impinging ethanol molecules in steps of 0.25 Å to ensure that the numerical evaluation of the free energy corresponded correctly to the analytical solution.

## III. Results and Discussion

In the following two sections we will examine the equilibrium structural properties of ethanol/$H_2O$ solutions as a function of concentration. In addition to pure $H_2O$ and pure ethanol, we have examined the following four ethanol/$H_2O$ solutions: $\chi_{ethanol} = 0.026$, $\chi_{ethanol} = 0.059$, $\chi_{ethanol} = 0.11$, and $\chi_{ethanol} = 0.40$. The first question we address is the accuracy of our ethanol/$H_2O$ model.

**A. Surface Tension.** Surface tension, or surface free energy ($\gamma$), is a measure of the degree of structure possessed by an interface. For example, at 298 K, the surface tensions of liquid $H_2O$[2] and liquid ethanol[3] are 72 and 22 dyn/cm, respectively. This difference reflects both the differences in the intermolecular forces that exist within the two bulk liquids and the hydrophobic nature of the of the liquid/vapor interface. Thus, to test if the SPC/E and OPLS/AA potential energy functions are correctly representing the liquid/vapor interface of an ethanol/$H_2O$ solution, we calculate surface tension as a function of ethanol concentration and compare our calculations to the existing experimental measurements.[3]

Using the theories of Kirkwood and Buff,[36−38] the surface tension of an aqueous solution can be determined in a MD simulation using the following equation:

$$\gamma = \frac{1}{2}\left\{\frac{1}{2A}\left\langle \sum_{i,j}\sum_{\alpha,\beta}\left(\frac{\partial V_{\alpha\beta}}{\partial r_{\alpha\beta}}\right)\left(\frac{1}{r_{\alpha\beta}}\right)(\vec{r}_{ij}\cdot\vec{r}_{\alpha\beta} - 3z_{ij}z_{\alpha\beta})\right\rangle\right\} \quad (4)$$

where $A$ is the area of the liquid/vapor interface, $V_{\alpha\beta}$ is the potential energy calculated between sites $\alpha$ and $\beta$ on molecules

**TABLE 3: Results of Fitting the *z*-Dependent Density Profiles of the $H_2O$ Molecules with the Hyberbolic Tangent Function Given in Eq 5[a]**

| $\chi_{ethanol}$ | $\rho_{water}$ (g/cm$^3$) | $z_{Gibbs}$[b] (Å) | $t$ (Å) | surface tension $\gamma$ (dyn/cm) |
|---|---|---|---|---|
| 0.00 | 1.002 | | 3.6 | 66 (±2) |
| 0.026 | 0.99 | ±17.08 | 4.3 (±0.1) | 61 (±1) |
| 0.059 | 0.94 | ±15.86 | 4.6 (±0.1) | 52 (±2) |
| 0.11 | 0.85 | ±14.94 | 5.1 (±0.1) | 44 (±2) |
| 0.40 | 0.38 | ±21.1 | 6.3 (±0.3) | 28 (±2) |
| 1.00 | | ±18.5 | 6.9 (±0.2) | 19 (±1) |

[a] In all cases, the temperature is maintained at 298 K and the *x* and *y* box dimensions are held constant at those values indicated in Table 2. The results of the surface tension calculations are also given. [b] The ± sign indicates that the simulation cell is centered at zero and that there are two interfaces: one at $+z_{Gibbs}$ and one at $-z_{Gibbs}$.

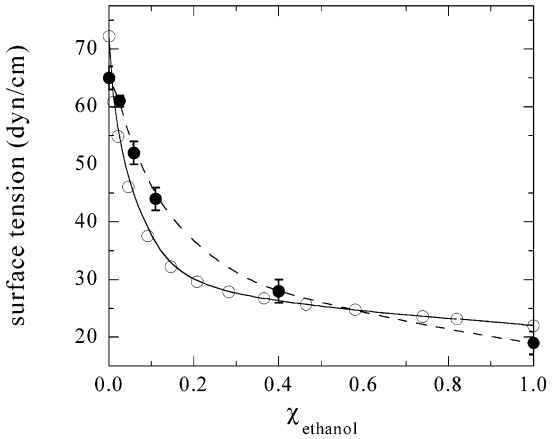


**Figure 2.** Surface tension of aqueous ethanol solutions as a function of ethanol concentration at 298 K. The open circles are the experimental data.[3] The closed circles are this work. The error bars represent one standard deviation of the simulation data. The dashed and solid lines are only meant as a guide for the eye.

*i* and *j*, $r_{\alpha\beta}$ and $z_{\alpha\beta}$ are the bond distance and the distance in the *z* direction between sites α and *β*, and $r_{ij}$ and $z_{ij}$ are the corresponding quantities calculated between the centers of mass of molecules *i* and *j*. The surface tension values calculated at 298 K for the ethanol solutions (closed circles) are given in Table 3 and shown in Figure 2 along with the corresponding experimental data (open circles).[3] The error bars represent one standard deviation calculated from 10 50 ps trajectories. The calculated surface tension of SPC/E water[24,25] and OPLS/AA ethanol[39] at 298 K are also shown in Figure 2. In agreement with the experimental data, our simulations predict that the surface tension of the solution decreases as the ethanol concentration increases. Although, enthalpy favors the total solution of the ethanol molecules into the bulk of the liquid, entropic forces push the ethanols toward the liquid/vapor interface. As shown in Figure 2, the surface tension of an aqueous ethanol solution is approximately that of bulk ethanol after the addition of only 0.2 mole fraction of ethanol.

Given the simplicity with which the SPC/E and OPLS/AA potentials treat $H_2O$ and ethanol molecules, respectively, and the fact that these two potentials were not developed to work together, the agreement between the MD simulations and the experimental data is quite good. The experimental surface tension[3] for pure ethanol is reported to be 22.03 dyn/cm whereas the value calculated using the OPLS/AA ethanol potential is 19 ± 1 dyn/cm. The comparison between the calculated and measured values is not as good at lower ethanol concentrations. At $\chi_{ethanol} = 0.11$, the calculated surface tension is 44 ± 2 dyn/cm compared to an experimental value of 38 dyn/cm. However, using the united-atom OPLS potential energy function for ethanol and the SPC/E model for water, Tarek and co-workers calculated the surface tension of their 0.10 mole fraction solution to be 54 dyn/cm.[13] Thus, we feel that, although the all-atom OPLS potential over-estimates the surface tension, it gives a better representation of the bonding in the ethanol film present on the surface of an aqueous ethanol solution than that provided by the OPLS united-atom potential energy function.

**B. Equilibrium Surface Structure.** *(a) Density Profiles.* The density profiles of the four ethanol/$H_2O$ solutions at 298 K are shown in Figure 3. These profiles are constructed by dividing the simulation cell shown in Figure 1 into 1.5 Å thick slabs along the *z* axis and subsequently calculating the $H_2O$ (open circles) and ethanol (closed circles) densities in each slab. By virtue of our simulation geometry, the $H_2O$ density profiles exhibit two interfaces with a plateau region in the middle that corresponds to the bulk portion of the solution. In all cases, the ethanol molecules preferentially reside at the solution/vapor interface (as indicated by the closed circles). Similar to Benjamin's work on DMSO/$H_2O$ solutions,[12] we do find a slight region of ethanol depletion and $H_2O$ enhancement just below the solution/vapor interface for the $\chi_{ethanol} = 0.40$ solution. However, for low ethanol concentrations ($\chi_{ethanol} \leq 0.11$), no depletion layer is found. These findings are in contrast to those of Tarek and co-workers, where an obvious depletion region of ethanol was noted for a 0.1 mole fraction ethanol solution.[13] The density profiles shown in Figure 3 are calculated from a 200 ps trajectory that is performed after at least 1 ns of prior equilibration time. However, the density profiles of Tarek and co-workers were calculated during the first 350 ps of equilibration time.[13] Recent work by Benjamin on the dynamic behavior of the surface equilibration process indicates that 350 ps is not adequate for the interface of an aqueous solution to attain its equilibrium structure.[12]

The $H_2O$ density profiles shown in Figure 3 are fit with a hyperbolic tangent function of the form[40]

$$\rho(z) = \frac{1}{2}(\rho_L + \rho_V) - \frac{1}{2}(\rho_L - \rho_V)\tanh\left[\frac{2.1972(z - z_0)}{t}\right] \quad (5)$$

where $\rho_L$ and $\rho_V$ are the densities of the bulk liquid and vapor phases, $z_0$ is the position of the Gibb's dividing surface, and *t* is the interface thickness (i.e., the thickness over which the density of the water changes from 90% $\rho_L$ to 10% $\rho_L$ assuming $\rho_V$ is equal to zero). The calculated $H_2O$ densities, interface thicknesses, and locations of the Gibb's interfaces are given in Table 3. As the concentration of ethanol increases, the density of $H_2O$ in the bulk solution decreases. This decrease is gradual for $\chi_{ethanol} \leq 0.11$ but becomes quite dramatic when the ethanol concentration changes from 0.11 to 0.40 mole fraction. The interface thickness also increases as the ethanol concentration increases. For the 0.026 ethanol mole fraction solution, the interface thickness is 0.7 Å larger than that for pure $H_2O$, indicating that even at this low concentration the presence of the ethanol molecules at the interface affects the underlying $H_2O$ structure. The location of the Gibb's interface reflects the different sizes of the simulation systems. We have provided the values of $z_{Gibbs}$ to give the reader some feel for the various sizes of the solution lamellas once the free surfaces have been allowed to equilibrate. In all cases, the distance between the two Gibb's interfaces is less by at least 2 Å than what is predicted from the equilibration of the bulk solution. (For these values refer to the *x* and *y* box dimensions given in Table 2.)

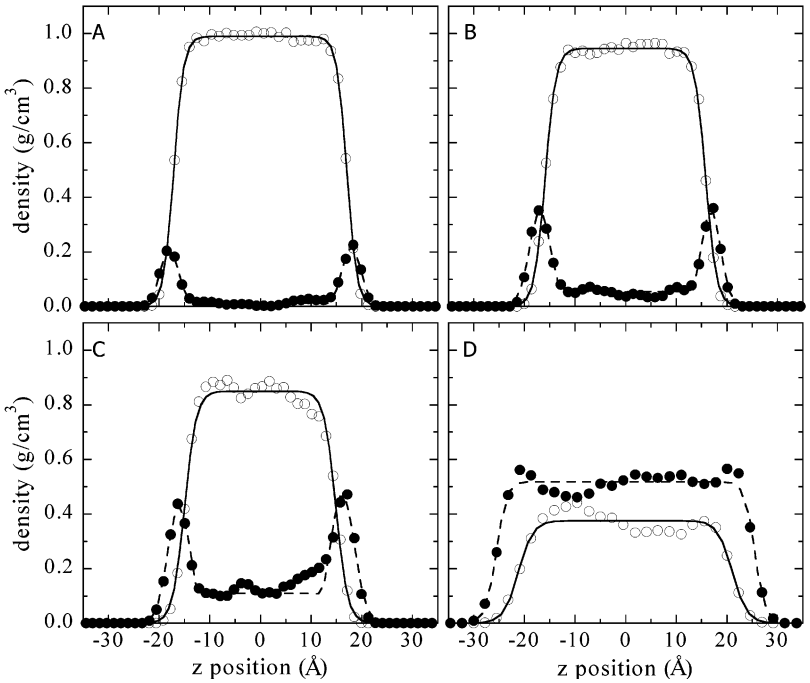


**Figure 3.** Density profiles of the four aqueous ethanol solutions at 298 K. Panels A−D correspond to $\chi_{ethanol} = 0.026$, 0.059, 0.11, and 0.40 solutions, respectively. The open circles represent the density profiles of the $H_2O$ molecules and the solid circles represent the density profiles of the ethanol molecules. The solid lines are the fits of the $H_2O$ data obtained with the hyperbolic tangent function given in eq 5. With the exception of panel D, the dashed lines are the fits to the ethanol data obtained with the Gaussian function given in eq 6 assuming a constant density of ethanol in the bulk of the solution. The ethanol distribution shown in panel D is fit with eq 5 (dashed line).

**TABLE 4: Results of Fitting the *z*-Dependent Density Profiles of the Ethanol Molecules with the Gaussian Function Given in Eq 6[a]**

| $\chi_{ethanol}$ | $z_{film}$[b] (Å) | $\sigma_e$ (Å) | $\Gamma_{ethanol}$ (mol/cm$^2$) (±0.5) |
|---|---|---|---|
| 0.026 | ±17.9 | 4.3 (±0.2) | $2.0 \times 10^{-10}$ |
| 0.059 | ±16.8 | 4.8 (±0.3) | $3.4 \times 10^{-10}$ |
| 0.11 | ±16.2 | 4.9 (±0.5) | $4.6 \times 10^{-10}$ |
| 0.40[c] | ±25.5 | 4.4 (±0.2) | $5.1 \times 10^{-10}$ |

[a] In all cases, the temperature is maintained at 298 K. Also shown is the calculated surface excess, $\Gamma_{ethanol}$. [b] The ± sign indicates that the simulation cell is centered at zero and that an excess of ethanol is found at each of the two interfaces: one at $+z_{film}$ and one at $-z_{film}$. [c] The ethanol distribution for the $\chi_{ethanol} = 0.40$ solution is not Gaussian in shape. It instead has the same shape as the water density distributions. Thus, its film position, $z_{film}$, and film thickness, $\sigma_e$, were calculated using the hyperbolic tangent function given in eq 5 and not the Gaussian function given in eq 6.

The ethanol density profiles for $\chi_{ethanol} \leq 0.11$ have been fit with the following Gaussian distribution assuming a constant ethanol density in the bulk of the solution:[13]

$$\rho_e(z) = \rho_e^0 \exp\left[\frac{-4(\ln 2)(z - z_{film})^2}{\sigma_e^2}\right] \quad (6)$$

where $\sigma_e$ and $z_{film}$ are the width and position of the ethanol excess, respectively. Within the error bars of our fits, no significant difference in the width of the excess as a function of concentration is found. Experiments report widths (after correcting for the surface roughness caused by capillary motion) of the ethanol excess of 6 and 4 Å for 0.022 and 0.10 ethanol mole fraction solutions, respectively.[8] Our values fall within this range. The ethanol distribution for the 0.40 mole fraction ethanol solution is not Gaussian in shape. It is instead better fit with the hyperbolic tangent function given in eq 5. Here, $\sigma_e$ (given in Table 4) is not the thickness of the ethanol excess but is instead the width over which the ethanol density decays from 90% to 10% of its bulk value. An equilibrated gas phase OPLS/AA ethanol molecule is approximately 4.1 Å in length.[26] Thus, this thickness and those found for $\chi_{ethanol} \leq 0.11$ are consistent with having a single monolayer of ethanol adsorbed at the solution liquid/vapor interface. The spatial distribution of ethanol molecules at the interface is not entirely uniform. For $\chi_{ethanol} \leq 0.059$, the interfacial ethanol molecules tend to cluster into small strands with the methylene carbon atoms of the nearest neighbor ethanol molecules approximately 5 Å apart.

The surface excess of ethanol, $\Gamma_{ethanol}$, is defined as[12]

$$\Gamma_{ethanol} = \frac{N_{ethanol} - \rho_{bulk} V}{S} \quad (7)$$

where $N_{ethanol}$ is the total number of ethanol molecules, $\rho_{bulk}$ is bulk number density of ethanol, $V$ is the volume enclosed by the two Gibbs' dividing surfaces (as defined by the $H_2O$ density profiles), and $S$ is the total surface area of the interface. (Because our simulation cell has two interfaces, the total surface area is twice the surface area of one interface.) The calculated values of $\Gamma_{ethanol}$ are given in Table 4. As expected for a surface active species, $\Gamma_{ethanol}$ is a positive number at all four concentrations. Experimentally, $\Gamma_{ethanol}$ ranges from $3.1(\pm0.3) \times 10^{-10}$ mol/cm$^2$ for $\chi_{ethanol} = 0.022$ to $5.9(\pm0.5) \times 10^{-10}$ mol/cm$^2$ for $\chi_{ethanol} = 0.10$.[8] Our calculated values are smaller than the experimental values. These differences, however, are consistent with those found between our calculated and the measured surface tension values. The thermodynamic properties of our simulated solutions correspond to solutions having lower concentrations. For example, the experimental values of $\gamma$[3] and $\Gamma_{ethanol}$[8] for a 0.045 ethanol mole fraction solution are 47 dyne/cm and $4.6 \times 10^{-10}$ mol/cm$^2$, respectively. These values are comparable to those we calculated for a 0.11 ethanol mole fraction solution.

*(b) Ethanol Orientations.* Figure 4 shows the orientational distributions for the ethanol molecules adsorbed at the solution/

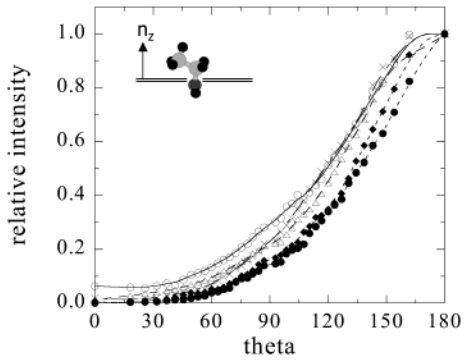


**Figure 4.** Average orientation of the ethanol molecules adsorbed at the solution/vapor interface relative to the surface normal, $n_z$, at 298 K. $\theta$ is the angle between $n_z$ and the C−O bond. $\chi_{ethanol} = 1.0$ (○), 0.40 (△), 0.11 (×), 0.059 (●), and 0.026 (◆). The lines are only meant as a guide for the eye. The inset depicts the typical orientation of an ethanol molecule adsorbed at the solution/vapor interface.

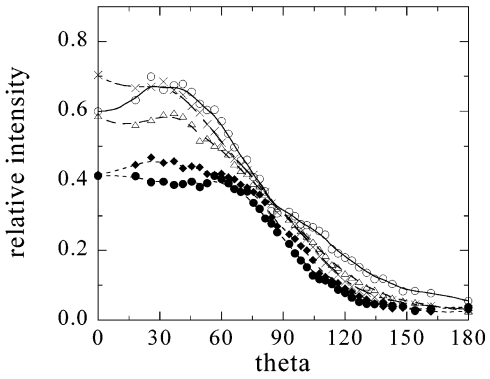


**Figure 5.** Average orientation of the ethanol molecules adsorbed at the solution/vapor interface relative to $n_z$. Here, $\theta$ is defined as the angle between $n_z$ and the C−C bond. The definitions of the symbols and lines are the same as that given in Figure 4.

vapor interface. In addition to the four aqueous solutions, orientational data is also provided for pure ethanol. The angle monitored is that between the surface normal and the C−O bond axis of ethanol. This angle can vary from 0° to 180° with an angle of 90° corresponding to the bond lying parallel to the plane of the surface. All five curves have been independently peak-normalized. In all cases, the hydrophilic end of the ethanol molecule points into the solution lamella, as indicated by the angle between the surface normal and the C−O bonds being peaked about $\theta$ equal to 180°. The C−O peak distribution is broader for the higher concentration and pure ethanol solutions (the open symbols in Figure 4) than for the lower concentration ethanol solutions (the closed symbols in Figure 4). This change in the width of the orientational distribution occurs because fewer molecules are competing for the finite number of surface sites in the lower concentrations. Thus, the individual ethanol molecules can minimize the interaction of their hydrophobic carbon chain with the underlying water molecules. At the higher ethanol concentrations, a competition exists between minimizing the interactions of the carbon chains with the underlying $H_2O$ molecules and packing as many ethanol molecules on the surface as possible. An increased ordering as a function of decreased bulk concentration was also reported in the experimental SFG measurements of aqueous methanol solutions.[7]

The orientational distributions for the angle $\theta$ between the C−C bond length (defined as the vector pointing from the methylene carbon to the methyl carbon) and the surface normal are shown in Figure 5. Again, this angle can vary from 0° to 180° with an angle of 0° corresponding to the C−C bond pointing into the vapor. Each curve in Figure 5 has been peak-normalized relative to its C−O curve in Figure 4. In all cases, the C−C bond of ethanol is broadly distributed around 45°. For the lower concentration solutions ($\chi_{ethanol} \leq 0.059$), instead of a peak in the distribution one finds a plateau region in the C−C orientational distribution between 0° and 70°. (If the C−O to surface normal bond angle is 180°, one would predict a C−C to surface normal bond angle of 70.5° if ethanol were to retain its single molecule equilibrium structure.) SFG experiments of pure ethanol report the orientational distribution of the C−C bond versus the surface normal to be less than 40° with a fwhm at 70°.[41] This is in good agreement with our calculations for pure ethanol where the most probable orientation is found at 42° (open circles). The maximum in C−C orientational distribution is also approximately 42° for the 0.11 and 0.40 mole fraction solutions. Given that their C−O orientation distribution curves are peaked about 180° relative to the surface normal, one possible explanation for a C−C bond angle of 42° is that the ethanol molecules have straightened (relative to their single molecule equilibrium structure) in an attempt to pack more molecules at the interface.

*(c) Water Orientations.* The orientational distribution of the $H_2O$ molecules at the liquid/vapor interface plays a large role in determining the reactivity of the interface. SHG and SFG experiments find that the dipole moment of $H_2O$ is slightly tilted inward toward the bulk liquid[42] and that 25% of the surface $H_2O$ molecules have a free OH bond that is pointed into the vapor,[43] respectively. It has been previously shown that the SPC/E potential model for $H_2O$ recovers both aspects of this structure of the $H_2O$ liquid/vapor interface.[25] Here, we are interested in determining how increasing the concentration of ethanol in the solution affects the orientation of the $H_2O$ molecules at the interface.

Figure 6 shows the orientational distributions for the $H_2O$ molecules at the solution/vapor interface as a function of ethanol concentration. $\theta$ is defined as the angle between the $H_2O$ dipole vector and the surface normal. This angle can vary from 0° to 180° with an angle of 90° corresponding to the dipole vector lying in the plane of the interface. Panel A corresponds to 0.026 mole fraction of ethanol. The structure of the $H_2O$ molecules at the interface is essentially the same as that found for pure SPC/E $H_2O$. In the interfacial region, two distinct orientations of the $H_2O$ molecules exist. On the vapor side of the interface, the most probable orientation corresponds to the $H_2O$ dipole directed out of the solution at an angle of 78° relative to the surface normal. On the liquid side of the interface, however, the $H_2O$ molecules are oriented such that their dipole is lying in the plane of the interface. As expected, no orientation preference is found for the $H_2O$ molecules in the bulk portion of the simulation cell. For a 0.059 mole fraction ethanol solution (panel B), the orientation of the $H_2O$ molecules on the vapor side of the interface is affected by the adsorbed ethanol layer. Here, the most probable angle between the $H_2O$ dipole and the surface normal is 67.5° as compared to 74° for pure water.[25] In contrast, the structure of the $H_2O$ molecules on the liquid side of the interface is in essence unaffected (89° versus 87° [25] and 101° versus 100° [25] for the surface minus 1.5 and 3.0 Å peaks, respectively). By $\chi_{ethanol} = 0.11$, the structure of the $H_2O$ molecules on both sides of the interface is changed. Finally, for $\chi_{ethanol} = 0.40$, the orientation of the surface $H_2O$ molecules (i.e., the outermost $H_2O$'s) has completely shifted such that the orientational distribution is now sharply peaked about 141.5° with no predominate orientation existing 3 Å below the interface.

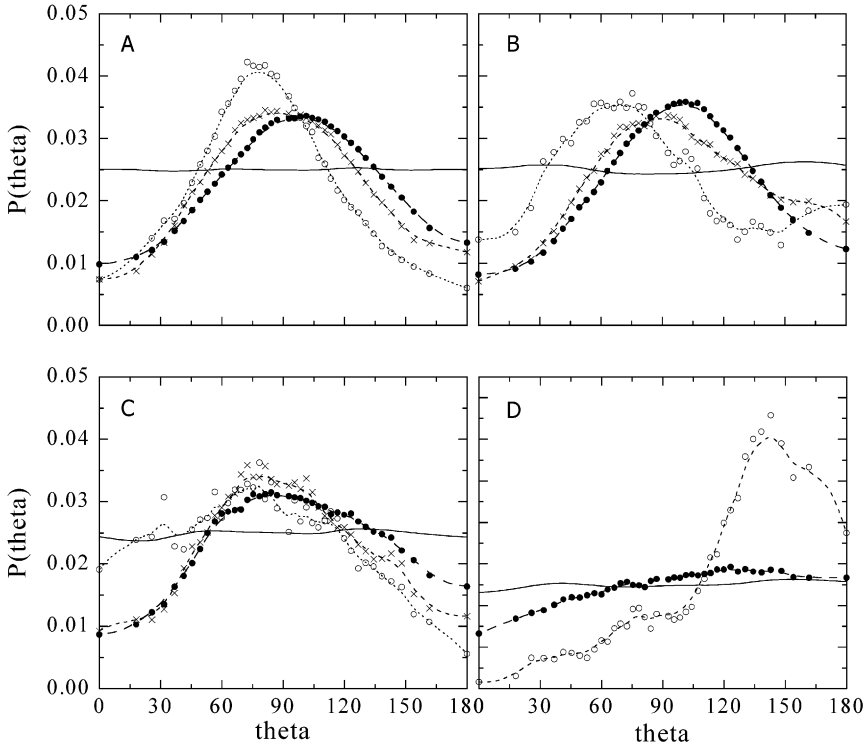


**Figure 6.** Average orientational distribution of the $H_2O$ dipole vector relative to the surface normal, $n_z$, as a function of concentration: (solid curve) orientation of the $H_2O$ molecules in the bulk of the solution; (●) orientation of the $H_2O$ molecules 3 Å from the surface; (×) orientation of the $H_2O$ molecules 1.5 Å from the surface; (○) orientation distribution of the $H_2O$ molecules at the surface. Panels A−D correspond to $\chi_{ethanol}$ = 0.026, 0.059, 0.11, and 0.40, respectively. The lines are a smooth fit to the data.

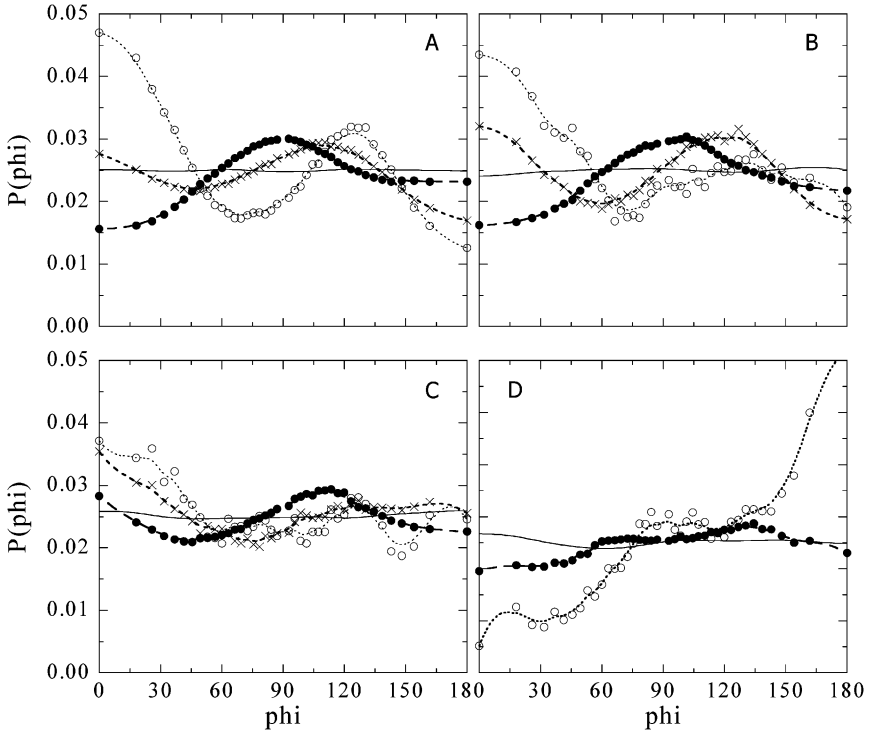


**Figure 7.** Orientation distribution of $H_2O$'s OH bond relative to the surface normal as a function of concentration. The definitions of the various symbols and panels are the same as that given in Figure 6.

As the concentration of ethanol is increased, the orientation of the vapor-side $H_2O$ molecules at first shifts to a smaller angle versus the surface normal and then rapidly shifts toward larger angles. As the ethanol concentration is increased from 0.026 to 0.059 mole fraction, the distribution of the $H_2O$ molecules has broadened and shifted to a smaller angle relative to the surface normal. This shift allows more ethanol molecules to adsorb in the finite number of available surface sites but yet maintains the highly structured nature of the $H_2O$ surface. However, as the concentration of ethanol molecules increases beyond $\chi_{ethanol}$ = 0.059, the highly ordered $H_2O$ structure is abandoned in choice of adsorbing more ethanol molecules at the interface. By $\chi_{ethanol}$ = 0.40, the $H_2O$ structure has completely changed to one in which the dipole moments of the $H_2O$ molecule are

pointing into the bulk liquid. This allows both the oxygen atom and perhaps one of the hydrogen atoms on the $H_2O$ molecules to hydrogen bond with the adsorbed ethanol molecules.

Figure 7 gives another view of the orientational distribution of the $H_2O$ molecules at the solution/vapor interface. Here, $\phi$ is defined as the angle between the O−H vector and the surface normal. Again, at $\chi_{ethanol} = 0.026$, the surface structure is very similar to that of pure $H_2O$ where $\phi$ is peaked at 0° and 120° for the outermost surface $H_2O$'s.[25] As the ethanol concentration approaches 0.40 mole fraction, this structure changes to one where the distribution of $\phi$ is sharply peaked at 180° versus the surface normal. Having the O−H bonds point 180° into the bulk, places the oxygen atoms in perfect position to hydrogen bond with the surface layer of ethanol molecules.

*(d) Hydrogen Bonding.* Below we have analyzed the effect of concentration on the $H_2O-H_2O$, ethanol−ethanol, and $H_2O$−ethanol hydrogen bonding structure. For DMSO−$H_2O$ solutions, Benjamin found that the number of $H_2O-H_2O$ hydrogen bonds monotonically decreased as the Gibb's surface was approached.[12] The degree of this decrease seemed to be independent of concentration. However, when he looked at the number of hydrogen bonds per $H_2O$ molecule divided by the $H_2O-H_2O$ coordination number, i.e., the fraction of *good* hydrogen bonds, Benjamin found that the degree of hydrogen bonding was affected more by the presence of the surface at lower DMSO concentrations than at higher DMSO concentrations.[12] Figure 8 shows a similar analysis of the $H_2O-H_2O$ hydrogen bonding as a function of concentration for ethanol/$H_2O$ solutions. In this analysis, we consider two molecules to be hydrogen-bonded if their O−O separation is less than 3.5 Å, their H−O separation is less than 2.6 Å, and their H−OH bond angle is greater than 140°. It has been demonstrated that the hydrogen bonding information obtained from this type of structural definition is similar to that obtained using a definition based upon the pair interaction energy.[12,13]

The top panel of Figure 8 shows the total number of $H_2O-H_2O$ hydrogen bonds per $H_2O$ molecules as a function of position along the *z* direction for the four solutions. The number of $H_2O-H_2O$ hydrogen bonds in the bulk region of the solution is inversely proportional to the ethanol concentration and decreases monotonically as the solution/vapor interface is approached. The lines are a fit of this monotonic decrease with the hyperbolic tangent function given in eq 5 where $\rho_V$ and $\rho_L$ are now defined as the number of hydrogen bonds per $H_2O$ molecule in the vapor phase and liquid phase, respectively. Although the fit of eq 5 to the hydrogen bonding data is not as good as its fit to the density data, it provides a qualitative picture of how the presence of the ethanol molecules affect the hydrogen bonding structure of the interfacial $H_2O$ molecules. Within the errors of the fits, no concentration dependence is found for the distance over which the number of hydrogen bonds per $H_2O$ molecule decays from 90% to 10% of its bulk value. (From the fits, distances of 9.8, 9.4, 9.9, and 10.3 Å are found for the 0.026, 0.059, 0.11, and 0.44 ethanol mole fraction solutions, respectively.)

The bottom panel in Figure 8 shows the fraction of *good* hydrogen bonds. This value is obtained by dividing the number of hydrogen bonds per $H_2O$ molecule by the average coordination number of $H_2O$ at a given depth. As in the DMSO work of Benjamin,[12] the probability of finding a *good* $H_2O-H_2O$ hydrogen bond increases as the concentration of ethanol increases. In the case of $\chi_{ethanol} = 0.026$ solution, approximately 88% of the bulk $H_2O-H_2O$ nearest-neighbor interactions are via hydrogen bonding. This number increases to 94% for the

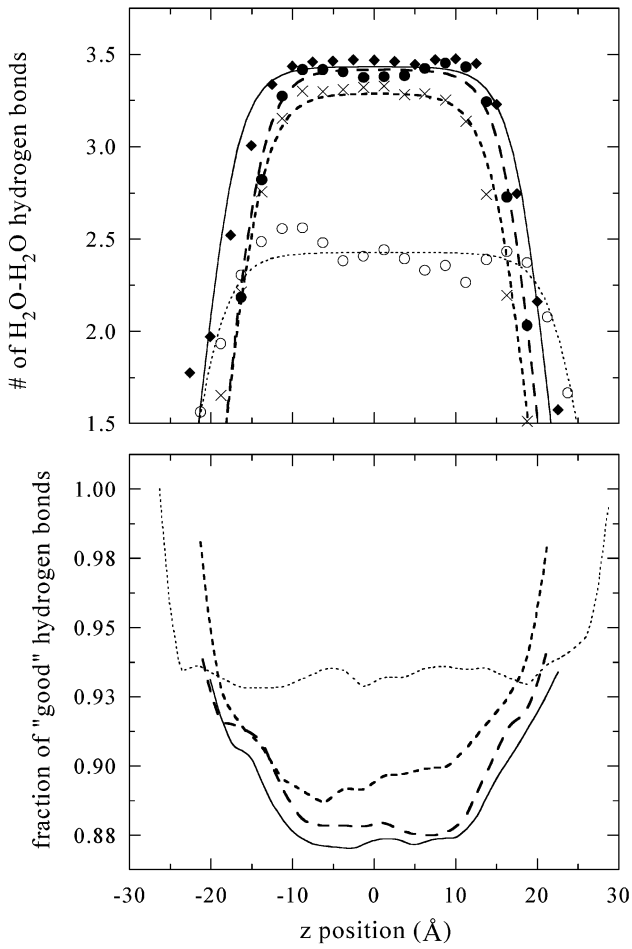


**Figure 8.** Top panel: number of $H_2O-H_2O$ hydrogen bonds per $H_2O$ molecule as a function of *z* position for the four aqueous ethanol solutions: $\chi_{ethanol} = 0.40$ (○), 0.11 (×), 0.059 (●), and 0.026 (◆). The lines are a fit to the hyperbolic tangent function given in eq 5. Bottom panel: number of $H_2O-H_2O$ hydrogen bonds per $H_2O$ molecule divided by the *z*-dependent coordination number of $H_2O$. The dotted, short dashed, long dashed, and solid lines correspond to $\chi_{ethanol} = 0.40$, 0.11, 0.058, and 0.026 solution, respectively. These lines are a smooth fit to the data.

$\chi_{ethanol} = 0.40$ solution. However, the effect of the interface is not as clear as that seen in the DMSO work. For all four solutions, the fraction of good hydrogen bonds does increase as the $H_2O$ molecules approach the surface. However, quantitatively, this fraction of *good* hydrogen bonds differs as a function of concentration. For the low concentrations ($\chi_{ethanol} \leq 0.059$), 93% of the $H_2O-H_2O$ nearest neighbor interactions at the interface are via hydrogen bonding; whereas, at the higher concentrations ($\chi_{ethanol} \leq 0.11$), 98% of the $H_2O-H_2O$ nearest neighbor interactions are via hydrogen bonding. Thus, the effect of the interface is less exact.

Figure 9 shows the number of ethanol-ethanol hydrogen bonds per ethanol molecule as a function of concentration. Here, we define two ethanol molecules to be hydrogen-bonded if the O−O separation is less than 3.5 Å, the O−H separation is less than 2.5 Å, and the H−OH bond angle is less than 140° (where H is the alcohol not the alkyl hydrogen of ethanol). This definition is similar to that used by Gao and Jorgensen in their examination of hexanol-hexanol hydrogen bonding at aqueous interfaces.[44] As the interface is approached an enhancement in the number of ethanol-ethanol hydrogen bonds is found. These numbers, however, are quite small with the maximum number approaching one ethanol-ethanol hydrogen bond for the 0.40 ethanol mole fraction solution. The orientation of the ethanol molecules at

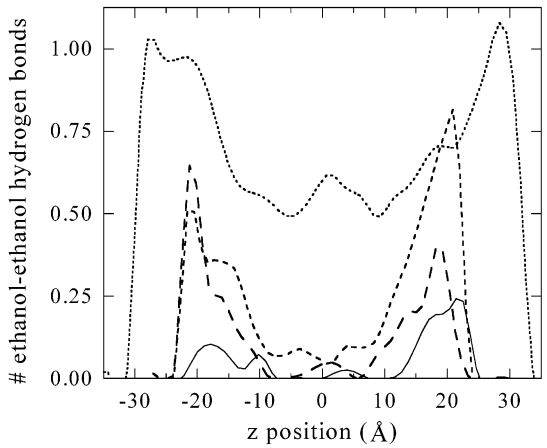


**Figure 9.** Number of ethanol−ethanol hydrogen bonds per ethanol molecule as a function of *z* position. The definitions of various lines types are same as that given for the bottom panel of Figure 8.

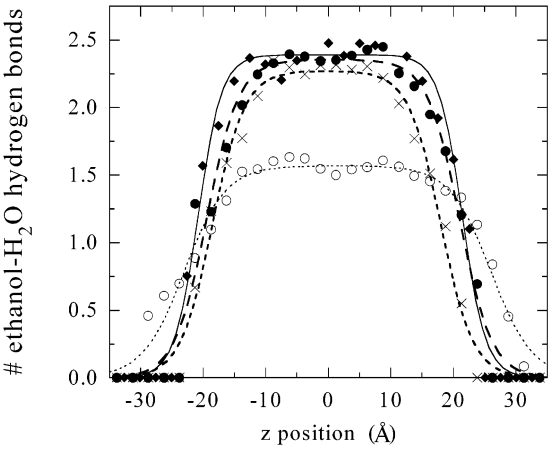


**Figure 10.** Distribution of ethanol−$H_2O$ hydrogen bonds per ethanol molecule. These data contain those hydrogen bonds where ethanol is acting both as a hydrogen acceptor and donor. $\chi_{ethanol} = 0.40$ (○), 0.11 (×), 0.059 (●), and 0.026 (◆). The lines are a fit to the hyperbolic tangent function given in eq 5.

the interface precludes more ethanol-ethanol hydrogen bonds from occurring.

The average number of ethanol−$H_2O$ hydrogen bonds per ethanol molecule as a function of distance from the interface is given in Figure 10. The same structural definition for a hydrogen bond as that given above is employed here. (Molecules with $O_{water}-H_{alcohol}$ and $O_{alcohol}-H_{water}$ separations less than 2.6 Å are further considered as possibly being hydrogen-bonded.) We see a monotonic decrease in ethanol−$H_2O$ hydrogen bonds as the interface is approached. This decrease is more pronounced for the lower ethanol concentrations than for the higher ethanol concentrations. If the information in Figures 9 and 10 is taken together, the total number of hydrogen bonds per ethanol molecule remains fairly constant for the $\chi_{ethanol} = 0.40$ solution but decreases from 2.2 hydrogen bonds per ethanol in the bulk to approximately 1.5 hydrogen bonds per ethanol at the interface for the $\chi_{ethanol} = 0.059$ solution.

As with the $H_2O-H_2O$ hydrogen bonding data, we have fit the ethanol−$H_2O$ hydrogen bond profiles with the hyperbolic tangent function given in eq 5. Although the individual fits to eq 5 are not good as the number of hydrogen bonds approaches zero, the errors systematically overestimate the thickness of the interface. Thus, these fits provide a qualitative picture of how the ethanol−$H_2O$ hydrogen bond profile is affected by the solution/vapor interface as a function of concentration. Figure

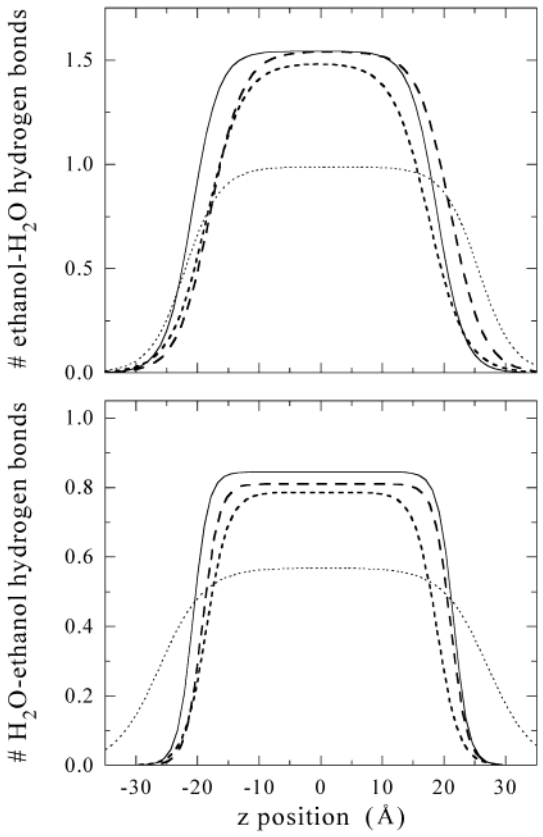


**Figure 11.** Distribution of ethanol−$H_2O$ hydrogen bonds per ethanol molecule. The top panel corresponds to those ethanol−$H_2O$ hydrogen bonds where ethanol is acting as the hydrogen acceptor and the bottom panel corresponds to those ethanol−$H_2O$ hydrogen bonds where ethanol is acting as the hydrogen donor. The line styles are defined in Figure 10 and are a fit of the data to the hyperbolic tangent function given in eq 5.

**TABLE 5: Distance Over Which the Number of Ethanol−$H_2O$ Hydrogen Bonds Per Ethanol Molecule Decays from 90% of Its Bulk Value to 10% of Its Bulk Value**[a]

| | ethanol−$H_2O$ hydrogen bonding '10-90' distance | |
|---|---|---|
| $\chi_{ethanol}$ | ethanol as H acceptor (Å) | ethanol as H donor (Å) |
| 0.026 | 9.6 | 5.5 |
| 0.059 | 11.7 | 5.9 |
| 0.11 | 12.9 | 7.8 |
| 0.40 | 12.5 | 15.9 |

[a] These distances were determined by fitting the ethanol−$H_2O$ hydrogen bonding profiles with eq 5.

11 shows the same data as that shown in Figure 10 but divides it into the number of ethanol−$H_2O$ hydrogen bonds per ethanol where ethanol is the hydrogen acceptor (top panel) and the number of $H_2O$−ethanol hydrogen bonds per ethanol where ethanol is the hydrogen donor (bottom panel). The interface thicknesses obtain from the fits of these data to eq 5 are given in Table 5. Again these thicknesses are only qualitatively correct. We quickly see, however, that for $\chi_{ethanol} \leq 0.11$ the ethanol−$H_2O$ hydrogen bonding structure decays from 90% to 10% of its bulk value over a longer distance when the ethanol molecule is the hydrogen donor than when the ethanol molecule is the hydrogen acceptor. Because a distinct orientation exists for the ethanol molecules at the interface, for an ethanol to be the hydrogen donor, the surface $H_2O$ molecules would need to orient themselves with their dipole vector pointing into the bulk solution. This is in direct contrast to what is found in pure $H_2O$.

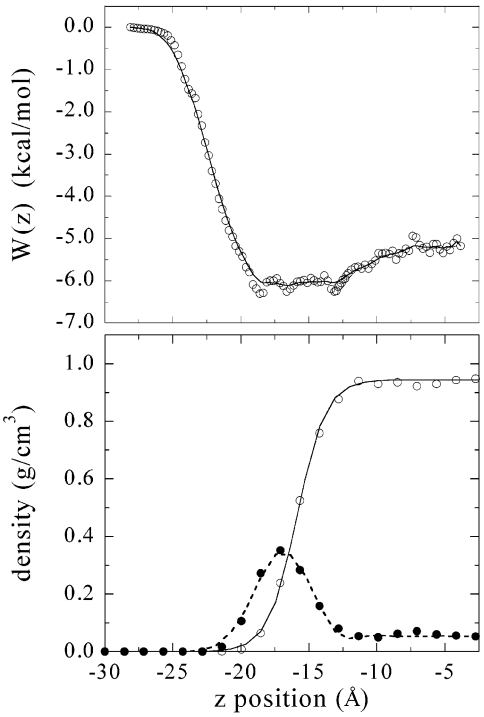


**Figure 12.** Top panel: free energy profile for the insertion of a single ethanol molecule into a $\chi_{ethanol} = 0.059$ mole fraction aqueous ethanol solution at 298 K. Bottom panel: corresponding region of the density profile for the $\chi_{ethanol} = 0.059$ ethanol solution through which the ethanol molecule is inserted. The open circles correspond to the $H_2O$ density profile and the closed circles correspond to the ethanol density profile.

Thus, the likelihood of finding an ethanol−$H_2O$ configuration of this sort at the interface is not high and the number of these types of ethanol−$H_2O$ hydrogen bonds quickly falls to zero. On the other hand, the orientation of the interfacial ethanol molecules does not adversely affect the possibility of forming an ethanol−hydrogen-acceptor ethanol−$H_2O$ hydrogen bond. Hence, at low concentrations, the idea that $H_2O$ molecules maintain their strong hydrogen bonding network at the expense of forming more ethanol−$H_2O$ interactions is reinforced. For $\chi_{ethanol} = 0.40$, ethanol's hydrogen donor curve (bottom panel) decays from 90% to 10% of the bulk value over a longer distance than its hydrogen acceptor curve (top panel). Here, packing more ethanol molecules at the interface becomes the governing force for determining the interfacial structure.

**C. Potential of Mean Force.** The free energy profile for the insertion of a single ethanol molecule into a $\chi_{ethanol} = 0.059$ ethanol/$H_2O$ solution has been calculated using the thermodynamic perturbation approach, and is shown in the top panel of Figure 12. The portion of the ethanol and $H_2O$ density profiles through which the molecule is inserted is shown in the lower panel of Figure 12. This density profile corresponds to that given in Figure 3B but shows only half of the range of *z*. The reaction coordinate is chosen to be the distance between the centers of mass of the impinging ethanol molecule and of the bulk solution, such that this coordinate is perpendicular to the solution/vapor interface. The zero of energy is defined to be when the impinging ethanol molecule is far (>10 Å) from the solution interface. The free energy for solvation, $\Delta G_{solv}$, is a measurement of the free-energy difference between a molecule being solvated in the bulk of the solution versus the molecule being in the gas phase. Thus, $\Delta G_{solv}$ can be measured directly from Figure 12 to have a value of −5.2 kcal/mol. The experimental value for $\Delta G_{solv}$ for an ethanol molecule in pure $H_2O$ is −5.0 kcal/mol.[45,46] This is very good agreement. As shown in the density profile for $\chi_{ethanol} = 0.059$ (bottom panel of Figure 12), the density of ethanol in the bulk of the solution is quite low (<0.1 g/cm$^3$), thus little difference should exist between $\Delta G_{solv}$ for an ethanol molecule in pure $H_2O$ and $\Delta G_{solv}$ for an ethanol molecule in a 0.059 mole fraction aqueous ethanol solution. Therefore, we feel confident that the potentials that we are employing provide a quantitative description of the energetics of the ethanol−$H_2O$ system.

As described earlier in the discussion of surface excess, ethanol is surface active and thus preferentially binds at the solution/vapor interface. This is confirmed by the broad minimum in the free energy profile between 13 and 18 Å. (The Gibb's interface for the bulk solution and the peak in the ethanol density are located at 15.86 and 16.8 Å, respectively.) The free energy for adsorption, $\Delta G_{ads}$, which is the calculated energy difference for an ethanol molecule being located in this interfacial minimum relative to the gas phase, is −6.1 kcal/mol. Thus, a +0.9 kcal/mol barrier exists between the surface site and the bulk solvation site (the difference between $\Delta G_{ads}$ and $\Delta G_{solv}$). No additional activation barrier, however, is found for the insertion of an ethanol molecule into a bulk $\chi_{ethanol} = 0.059$ aqueous ethanol solution. The lack of a large barrier between the surface site and the bulk solvated site is in agreement with our previous calculations for the insertion of a single ethanol molecule into bulk $H_2O$[15,16] but is in definite disagreement with the ideas of the resistance model.[20,21]

Within the resistance model, the mass-accommodation coefficient, α, for the insertion of an ethanol molecule into the bulk of a solution can be calculated via[21]

$$\frac{\alpha}{1-\alpha} = \frac{\exp\left(-\frac{\Delta G^{\ddagger}_{solv}}{RT}\right)}{\exp\left(-\frac{\Delta G_{desorb}}{RT}\right)} \qquad (8)$$

where $\Delta G_{desorb}$ is equal to $-\Delta G_{adsorb}$, $\Delta G^{\ddagger}_{solv}$ is equal to ($\Delta G_{solv} - \Delta G_{adsorb}$) when no activation barrier is present, *T* is the temperature in Kelvin, and *R* is the gas constant. Given our values for $\Delta G_{adsorb}$ and $\Delta G_{solv}$, the mass accommodation coefficient for inserting an ethanol molecule into a 0.059 mole fraction ethanol solution is 1.0 at 298 K. The experimental value for the mass accommodation coefficient for inserting an ethanol molecule into a dilute ethanol/$H_2O$ droplet is 0.0093 at 298 K.[20] Previously, we hypothesized that the difference between the experimental value of α and that calculated in our simulations might be due to the fact that the experimental model only allowed the impinging ethanol molecule to interact with a *clean* $H_2O$ surface.[15] However, given the surface activity of ethanol in aqueous solutions, real ethanol/$H_2O$ solutions have a *film* of ethanol on them through which the impinging ethanol molecule would need to traverse before becoming solvated in the bulk solution. Our current findings suggest that the existence of such a film is *not* the difference between the experiments and simulations and that a more fundamental difference exists between the mass accommodation coefficients being measured in the experiments and those being calculated via the MD simulations within the resistance model. What this fundamental difference is deserves further exploration.

## IV. Summary and Conclusions

Molecular dynamics computer simulations have been used to explore both the structure of the liquid/vapor interface of ethanol/$H_2O$ solutions as a function of concentration and to calculate the mass accommodation coefficient for the insertion

of an ethanol molecule into a $\chi_{ethanol} = 0.059$ aqueous ethanol solution. Using a combination of the SPC/E $H_2O$ potential[23] and the OPLS/AA ethanol potential,[26] we have been able to reproduce the experimental surface tension results as a function of concentration. In addition, the calculated free energy for solvation in the bulk liquid and the average orientation of ethanol molecules at the solution/vapor interface agree well with the corresponding experimental data. Thus, we believe that this combination of potential functions adequately describes the aqueous ethanol solution/vapor interface. At all concentrations, ethanol is found to be surface active. Ethanol molecules sit at the surface with their hydrophobic alkyl tails pointing into the vapor and their hydrophilic alcohol groups pointing into the solution. Below $\chi_{ethanol} = 0.11$, the orientation of the surface $H_2O$ molecules seems to be unaffected by the presence of the surface ethanol molecules. However, above $\chi_{ethanol} = 0.11$, the structure of the underlying $H_2O$ molecules is greatly changed. This may have measurable affects on the surface reactivity and solvation properties of these interfaces.

Below $\chi_{ethanol} = 0.11$, the distance over which the number of ethanol$-H_2O$ hydrogen bonds decays from 90% to 10% of the bulk number is longer for those hydrogen bonds where ethanol is the hydrogen acceptor as compared to when ethanol is the hydrogen donor. The opposite effect is seen for the 0.40 ethanol mole fraction solution. Together with the ethanol and $H_2O$ orientation data, this seems to support the idea that at low ethanol concentrations maintaining the strong $H_2O-H_2O$ hydrogen bonding network is the governing force in determining the interfacial structure. While at higher ethanol concentrations, where the orientation of the surface $H_2O$ molecules is opposite to that found in pure $H_2O$, the need to pack more ethanol molecules at the hydrophobic liquid/vapor interface becomes the dominant force.

Finally, the mass accommodation coefficient calculated for the insertion of a single ethanol molecule through the ethanol excess and into the bulk of an aqueous ethanol solution remains in disagreement with the experimental measurements of the mass accommodation coefficient.

**Acknowledgment.** We thank Drs. Liem X. Dang, Gregory K. Schenter, Bruce C. Garrett, and Ilan Benjamin for insightful discussions. We also thank the following organizations for their support of this work: Dreyfus Foundation (Grant # SU-97-048), the Research Corp. (Grant # CC5158), and the American Chemical Society, Petroleum Research Fund (ACS-PRF Grant # 36806-GB6).

## References and Notes

(1) Schwarzenbach, R. P.; Gschwend, P. M.; Imboden, D. M. *Environmental Organic Chemistry*; John Wiley & Sons: New York, 1993; pp 56−254.
(2) MacRitchie, F. *Chemistry at Interfaces*; Academic Press: New York, 1990; pp 12−23, 32−38.
(3) Schofield, R. K.; Rideal, E. K. *Proc. R. Soc. London* **1925**, *A109*, 60.
(4) Eisenthal, K. B. *Chem. Rev.* **1996**, *96*, 1343.
(5) Gragson, D. E.; Richmond, G. L. *J. Phys. Chem. B* **1998**, *102*, 3847.
(6) Miranda, P. B.; Shen, Y. R. *J. Phys. Chem. B* **1999**, *103*, 3292.
(7) Wolfrum, K.; Graener, H.; Laubereau, A. *Chem. Phys. Lett.* **1993**, *213*, 41.
(8) Li, Z. X.; Lu, J. R.; Styrkas, D. A.; Thomas, R. K.; Rennie, A. R.; Penfold, J. *Mol. Phys.* **1993**, *80*, 925.
(9) Matsumoto, M.; Kataoka, Y. *J. Chem. Phys.* **1989**, *90*, 2398.
(10) Matsumoto, M.; Takaoka, Y.; Kataoka, Y. *J. Chem. Phys.* **1993**, *98*, 1464.
(11) Benjamin, I. *Chem. Rev.* **1996**, *96*, 1449.
(12) Benjamin, I. *J. Chem. Phys.* **1999**, *110*, 8070.
(13) Tarek, M.; Tobias, D. J.; Klein, M. L. *J. Chem. Soc., Faraday Trans.* **1996**, *92*, 559.
(14) Taylor, R. S.; Ray, D.; Garrett, B. C. *J. Phys. Chem. B* **1997**, *101*, 5473.
(15) Taylor, R. S.; Garrett, B. C. *J. Phys. Chem. B* **1999**, *103*, 844.
(16) Wilson, M. A.; Pohorille, A. *J. Phys. Chem. B* **1997**, *101*, 3130.
(17) Somasundaram, T.; Lynden-Bell, R. M.; Patterson, C. H. *Phys. Chem. Chem. Phys.* **1999**, *1*, 143.
(18) Mountain, R. D. *J. Phys. Chem. B* **2001**, *105*, 6556.
(19) Dang, L. X.; Chang, T.-M. *J. Phys. Chem. B.* **2002**, *106*, 235.
(20) Jayne, J. T.; Duan, S. X.; Davidovits, P.; Worsnop, D. R.; Zahniser, M. S.; Kolb, C. E. *J. Phys. Chem.* **1991**, *95*, 6329.
(21) Nathanson, G. M.; Davidovits, P.; Worsnop, D. R.; Kolb, C. E. *J. Phys. Chem.* **1996**, *100*, 13007.
(22) Donaldson, D. J.; Anderson, D. *J. Phys. Chem. A* **1999**, *103*, 871.
(23) Berendsen, H. J. C.; Gigera, J. R.; Straatsma, T. P. *J. Phys. Chem.* **1987**, *91*, 6269.
(24) Alejandre, J.; Tildesley, D. J.; Chapela, G. A. *J. Chem. Phys.* **1995**, *102*, 4574.
(25) Taylor, R. S.; Dang, L. X.; Garrett, B. C. *J. Phys. Chem.* **1996**, *100*, 11720.
(26) Jorgensen, W. L.; Maxwell, D. S.; Tirado-Rives, J. *J. Am. Chem. Soc.* **1996**, *118*, 11225.
(27) Allen, M. P.; Tildesley, D. J. *Computer Simulations of Liquids*; Oxford University Press: New York, 1987.
(28) Pearlman, D. A.; Case, D. A.; Caldwell, J. C.; Seibel, G. L.; Singh, U. C.; Weiner, P.; Kollman, P. *AMBER*, 4.0 ed.; University of California: San Francisco, CA 1991.
(29) Verlet, L. *Phys. Rev.* **1967**, *159*, 98.
(30) Berendsen, H. J. C.; Postama, J. P. M.; van Gunsteren, W. F.; DiNola, A.; Haak, J. R. *J. Chem. Phys.* **1980**, *72*, 2384.
(31) Ryckaert, J. −P.; Ciccotti, G.; Berendsen, H. J. C. *J. Comput. Phys.* **1977**, *23*, 327.
(32) Kirkwood, J. G. *J. Chem. Phys.* **1930**, *3*, 300.
(33) Zwanzig, R. W. *Chem. Phys.* **1954**, *22*, 1420.
(34) Huston, S. E.; Rossky, P. J.; Aichi, D. A. *J. Am. Chem. Soc.* **1989**, *111*, 5680.
(35) Smith, D. E.; Dang, L. X. *J. Chem. Phys.* **1994**, *100*, 3757.
(36) Fowler, R. H. *Proc. R. Soc.* **1937**, *A159*, 229.
(37) Kirkwood, J. G.; Buff, F. P. *J. Chem. Phys.* **1949**, *17*, 338.
(38) Salomons, E.; Mareschal, M. *J. Phys.: Condens. Matter* **1991**, *3*, 3645.
(39) Taylor, R. S. Manuscript in preparation.
(40) Townsend, R. M.; Rice, S. A. *J. Chem. Phys.* **1985**, *82*, 4391.
(41) Stanners, C. D.; Du, Q.; Chen, R. P.; Cremer, P.; Somorjai, G. A.; Shen, Y. R. *Chem. Phys. Lett.* **1995**, *232*, 407.
(42) Goh, M. C.; Hicks, J. M.; Kemnitz, K.; Pinto, G. R.; Bhattacharyya, K.; Eisenthal, K. B.; Heinz, T. F. *J. Phys. Chem.* **1988**, *92*, 5074.
(43) Du, Q.; Freysz, E.; Shen, Y. R. *Science* **1994**, *264*, 826.
(44) Gao, J.; Jorgensen, W. L. *J. Phys. Chem.* **1988**, *92*, 5813.
(45) Cabani, S.; Gianni, P.; Mollica, V.; Lepori, L. *J. Solution Chem.* **1981**, *10*, 563.
(46) Ben-Naim, A.; Marcus, Y. *J. Chem. Phys.* **1984**, *81*, 2016.